Study on the External Surface Acidity of MCM-22 Zeolite: Theoretical Calculation and ^{31}P MAS NMR

Yan Wang, Jianqin Zhuang, Gang Yang, Danhong Zhou, Ding Ma, Xiuwen Han, and Xinhe Bao*

State Key Laboratory of Catalysis, Dalian Institute of Chemical Physics, Chinese Academy of Sciences, Dalian, 116023 Liaoning, China

Received: April 12, 2003; In Final Form: November 18, 2003

The acidity on the external surface of the MCM-22 zeolite was studied by theoretical calculations combined with a magic angle spinning (MAS) NMR experiment. The ^{31}P MAS NMR spectrum of triphenylphosphine (PPh_3) adsorbed on the MCM-22 zeolite and the XRF (X-ray fluorescence) element analysis showed that there were about 6% Brønsted acidic sites distributed on the external surface. During theoretical calculations, PPh_3 was used as the probe molecule to further study the nature of interaction. Periodic molecular mechanical simulations revealed that the probe molecule preferred to adsorb on the 12 MR external surface pockets of the MCM-22 zeolite and was too large to enter completely into the surface pockets. It preferred to locate at the openings of external surface pockets, with one alkyl inserting into the pockets of the supercage, whereas the others remained in the outside, which confirmed the result that only 6% Brønsted acid sites were detectable by ^{31}P MAS NMR using PPh_3 as the probe molecule. Moreover, periodic MM calculation indicated that PPh_3 was able to adsorb on T1 and T4 sites, which were the most possible sites for the Al introduced into the zeolite lattice. The existence of two Brønsted-bound PPh_3 peaks at 11.1 and 14.8 ppm in the ^{31}P MAS NMR spectrum was strongly supported by the above theoretical results. Thus, the molecular mechanical simulation not only provided structural support to the interpretation of NMR experiment but also perfectly agreed with the results from ^{31}P MAS NMR measurements. The structures and interaction energies of the acid−base complexes were further calculated by DFT method. The quantum mechanical calculations indicated that the protonic H atoms of the MCM-22 zeolite were transferred to the probe molecules, resulting in the "ionic" structure, which was in good agreement with the result of Lunsford etc. Because the Brønsted acidity was associated with the ability of transferring proton, the calculation results can give a qualitative understanding of the acidic strength at the openings of the external surface pockets of the MCM-22 zeolite. The effects of the cluster model and the functional level were also discussed in detail.

1. Introduction

Zeolite MCM-22,[1] a recently synthesized zeolite species, consists of two independent channel systems: a 10-MR (member ring) sinusoidal (4.0 × 5.9 Å diameters) and a 12-MR supercages (7.1 × 18.1 Å) interconnected through 10-MR windows.[2] Due to the characteristic pore systems, MCM-22 has been widely used as catalysts for many kinds of reactions, such as isomerization, cracking, and other synthesis reactions.[3−6]

Up to now, a great deal of work has been done on the study of structural, adsorptive and catalytic properties of MCM-22 zeolite.[7−15] Several reports showed that the shape selectivity of MCM-22 zeolite is intermediate between that of 10- and 12-member ring zeolites, indicating that external surface acid sites are contributing to the catalytic conversion.[9,12] Cheng et al. proposed an external surface reaction mechanism by considering that the 12-MR pockets on the external surface of MCM-22 crystals may play a dominant role in some catalytic processes.[13] However, the detailed studies of the distribution and strength of the Brønsted acid site on the 12-MR external surface pocket of MCM-22 are rather limited. The MCM-22 zeolite is very small crystallites, and its external surface mainly consists of 12-MR external surface pockets. Many molecules that are too large to penetrate through the 10-MR channels have been used to explore the important role of the external surface.[16,17] Among them, some molecules such as 1,3,5-triisopropylbenzene, with a dynamic diameter not only larger than the 10-MR channels but also larger than the 12-MR external surface pockets, can detect the acidity on the external surface of MCM-22 zeolite.[18]

The ^{31}P magic angle spinning (MAS) NMR technique is very useful to investigate the acidity of zeolites. Various organophosphorus compounds were used as probe molecules to reveal the interaction between the probe molecules and the Brønsted acid sites.[19−23] Theoretical calculations also play a very important role in studying the acidity of zeolites. However, compared with other zeolites, theoretical studies on the acidity of MCM-22 are rather limited. By using two different force fields, Sastre[24] et al. reported that a stronger acidity was predicted for the centers located in the supercages of the MCM-22 zeolite with respect to those in the sinusoidal channels. Recently, by using quantum mechanical, Zhou et al.[25,26] concluded that the T1 and T4 sites located at the openings of the 12-MR external surface pockets of the MCM-22 zeolite were the most preferable locations for aluminum substitution.

In the present work, the external surface acidity of MCM-22 zeolite was characterized by triphenylphosphine (PPh_3) adsorp-

* Corresponding author. Tel: 086-0411-4686637. Fax: 086-0411-4694447. E-mail: xhbao@dicp.ac.cn.

10.1021/jp034989y CCC: $27.50
Published on Web 12/30/2003

tion followed by a ^{31}P MAS NMR spectrum. The main advantage of PPh_3 is that its molecular size (11.7×7.1 Å)[27] is larger than the 12-MR external surface pockets (7.1×9.2 Å) just as 1,3,5-triisopropylbenzene. Thus it can be used to detect the special acid sites on the external surface of the MCM-22 zeolite. Theoretical calculations were further performed to study the nature of the interaction between the probe molecules and the MCM-22 zeolite. In our calculations, the possible locations and the acidity of the Brønsted acid on the external surface of MCM-22 zeolite were estimated. The effects of the cluster model and the functional level on the calculated results were also discussed.

2. Experimental Section

MCM-22 zeolite with a SiO_2/Al_2O_3 ratio of 32 was synthesized according to the preparation method reported in the literature.[28] The sample was put into a U-type tube, and dehydrated at 773 K for 6 h under pure helium (99.99%) atmosphere and with a flow rate of 20 mL/min. Then, PPh_3 vapor was adsorbed on the samples at 423K for 2 h. After cooling to room temperature, the samples were transferred into a 4 mm ZrO_2 MAS NMR rotor and sealed with a cap under He environment.

NMR measurement was carried out at room temperature on a Bruker DRX-400 spectrometer with a BBO MAS probehead. ^{31}P MAS NMR spectra with high-power proton decoupling were performed at 161.9 MHz, using a 2.0 μs pulse, a 2 s repetition time, and 4096 scans. The sample was spun at 6 kHz and chemical shifts were referenced to 85% H_3PO_4. The recycle time in our experiments was long enough to obtain quantitative peak intensities. Combining ^{31}P MAS NMR and XRF (X-ray fluorescence) elemental analysis, the amount of detectable external surface acidity could be determined.

3. Methodology and Model

To obtain exact and detailed information about the interaction between the probe molecules and the zeolite lattice, a two-step calculation combining molecular and quantum mechanical calculations was carried out.[29−31] The preferred adsorption sites of the probes molecules on MCM-22 zeolite were first obtained by periodic molecular mechanical simulation, and then quantum mechanical approach using a cluster approximation was implemented for further study. Periodic molecular mechanical calculation has been carried out by fully optimizing the cell parameters and the atomic coordinates of all the atoms in the MCM-22 unit cell. The convergence criterion of a gradient norm below 0.001 ev/Å was used in the geometry optimization. PPh_3 has been introduced in each of the topologically different environments in MCM-22 zeolite. The force-field used includes two-body interatomic interactions. To investigate the dependence of the calculation results on the cluster models in DFT simulations, two different cluster models were chosen. The first cluster model $H_3Si-HO-Al(OSiH_3)_3$ consisted of 5T (Si, Al) atoms, and the Al atom was the center of the cluster. The other cluster model $(H_3SiO)_3Si-HO-Al(OSiH_3)_3$ possessed 8T (Si, Al) atoms, and the O atom was the center of the cluster. These two clusters were referred to as model A and model B, respectively. The dangling silicon bonds were terminated with hydrogen atoms with a distance of 1.4 Å to the connected framework Si atoms. During the optimization process, the outermost two coordination shells of clusters were fixed in their crystallographic positions, whereas the rest of the clusters and the probe molecules were fully optimized. The T4 site was chosen to represent the preferable site of Al substitution and the reason will be discussed in more detail later. The crystallographic labeling of pure silica MCM-22 is in accordance with the *Atlas* of the zeolite structure[32] and is shown in Figure 1.

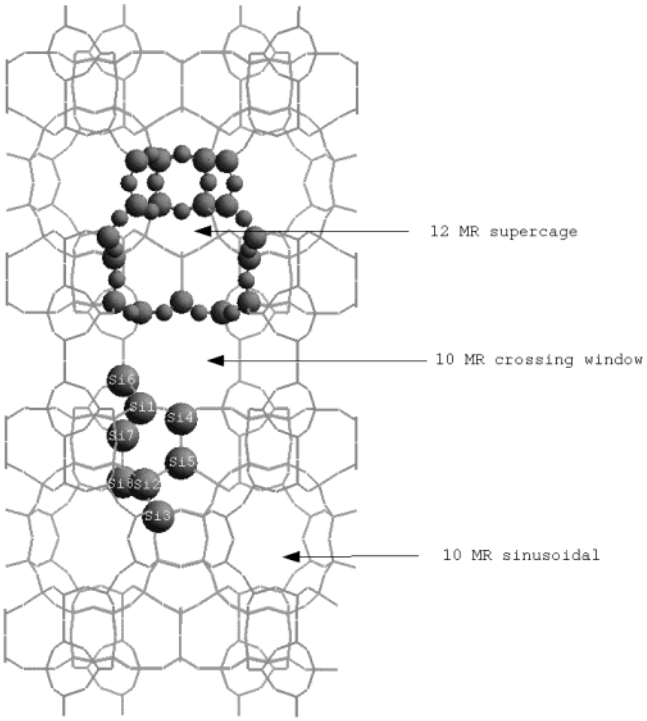

Figure 1. Structure of MCM-22 showing the eight different T sites. The crystallographic labeling of pure silica MCM-22 is in accordance with that in the Atlas of zeolite.[32]

Periodic molecular mechanical simulations and quantum mechanical calculations in this work were performed in Cerius2.[33] In periodic molecular mechanical simulations, the Burchart1.01-Dreiding2.21 force field (MSI 1997)[34] was applied. This force field combines the Burchart1.01 and DREIDING2.21 force field. The Burchart1.01 force field was used to treat the framework, whereas the DREIDING2.21 force field was used to handle the intra- and intermolecular interactions. In the quantum mechanical calculations, the density functional method (DFT) was used. The calculations were performed at two levels of functionals to the exchange-correlation potential, namely, the local PWC functional and the nonlocal BLYP functional. A double numerical with polarization (DNP) basis set was performed. The DNP basis sets are comparable in size to the commonly used 6-31** Gaussian orbital basis set.[35,36] However, the numerical basis set is much more accurate than a Gaussian basis set with the same size.

4. Results and Discussion

4.1. ^{31}P MAS NMR Experiment. The ^{31}P MAS NMR spectrum of PPh_3 adsorbed on MCM-22 zeolites ($SiO_2/Al_2O_3 = 32$) is shown in Figure 2. The resonance at −4.6 ppm was assigned to physisorbed phosphine. The peaks at lower field with chemical shifts at 11.1 and 14.8 ppm were both related to Brønsted-bound PPh_3, which arose from the protonation of the PPh_3 at Brønsted acid sites on the external surface of the MCM-22 zeolite.[37] The peak for Lewis acid sites was not observed because its shift was close to that of the physisorbed phosphine. On the basis of the result of XRF element analysis and peak simulation of ^{31}P MAS NMR spectrum, about 6% Brønsted acid sites (relative to the total acid sites of the sample) were detected. As we have stated above, because the size of PPh_3 is larger than that of the 12-MR surface pocket, the ^{31}P MAS NMR

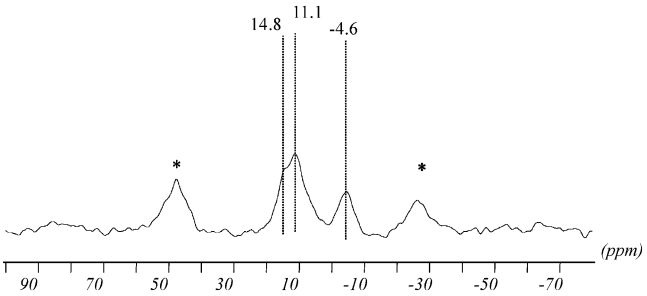

Figure 2. ^{31}P MAS NMR spectrum of PPh_3 adsorbed on HMCM-22 zeolite.

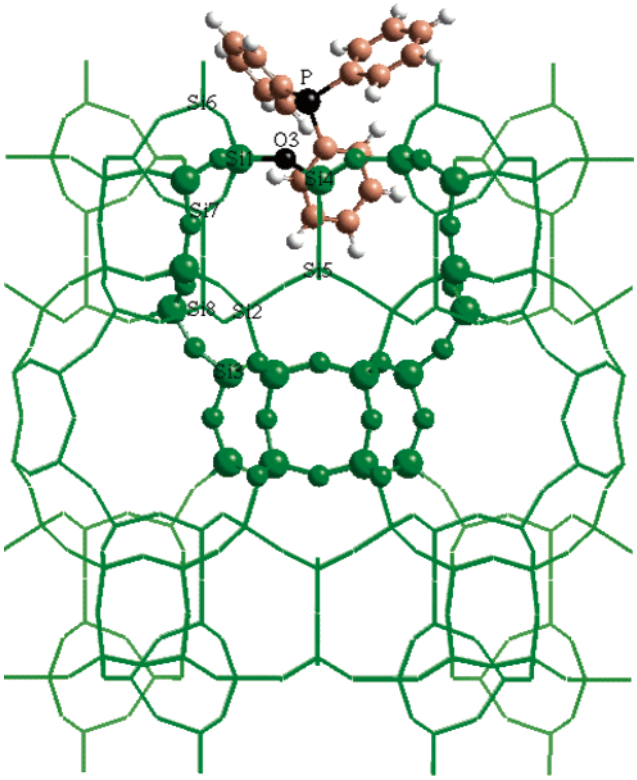

Figure 3. Local map showing the structure of the sorption of PPh_3 at the MCM-22 zeolite unit cell with minimum energy.

experiment only detected a portion of the Brønsted acid sites at the external surface pocket of the MCM-22 zeolite. Thus, further research is needed to clarify which part of an external surface pocket the PPh_3 molecule interacted with and how they interacted with each other. In the following section, theoretical calculations will be employed to answer these questions.

4.2. Molecular Mechanical Calculation. In our theoretical calculations, a molecular mechanical simulation was carried out first. With the molecular mechanical treatment, many initial configurations of the system were specified and the interatomic distances and bond angles were adjusted using an iterative method, until a minimum energy configuration was obtained for the system. In a simulation of zeolite, it is very important to choose the appropriate force field. In this work, the Burchart1.01-Dreiding2.21 force field was chosen. There have been many studies on the adsorption of organic molecules on zeolites using this force field.[38] By simulation, it was found that PPh_3 was definitely too large to completely enter into the pores of the MCM-22 zeolite once the minimum energy state was attained and a local map which showed the structure was enlarged and shown in Figure 3. Because there was much room between the two-half supercages and the effect of the electrostatics of the fully surrounding pore system was little different from that when only a semi-infinite pore environment was present, the simulation result was extrapolated such that the probe molecule would also not fully enter a surface pocket and preferred to locate at the opening of 12-MR pocket, with one alkyl group inserting into the pocket. The result was similar to the adsorption of monobranched alkanes on ZSM-22 zeolite. The branched alkanes would lie mainly at the pore mouth, with their longest linear alkyl group going into the ZSM-22 pore, whereas the other shorter alkyl groups remained outside.[39] According to crystallographic labeling of pure silica MCM-22, all the T sites at the opening of external surface pocket are T1 and T4 sites. Thus, the result by periodic MM simulation was coincident with the one of our previous theoretical calculations.[25,26] By calculating the substitution energy, the proton affinity, the acidity strength of different oxygen bridge, and the frequency of the O−H bond, it was confirmed that the preferable Al substitution sites were T1 and T4 sites at the openings of the pocket. On the basis of the above discussion, we drew a conclusion that the 6% Brønsted acids detected by the ^{31}P MAS NMR experiment mainly arose from the Brønsted acid at the openings of the external surface pockets of MCM-22.

Thus, by using the periodic MM simulation, the preferred adsorption sites of the probe molecule were well-defined and the NMR experiment result was successfully explained. Moreover, there was a perfect match between NMR experiment and theoretical calculation. First, the calculation result has concluded that only parts of the acid sites are accessible to large probe molecules, consistent with the experimental result that only 6% Brønsted acid sites are detectable by ^{31}P MAS NMR using PPh_3 as the probe. Second, the periodic MM calculation indicates that PPh_3 is able to adsorb on T1 and T4 sites, which are the most possible sites for the Al introduced into the zeolite lattice. The existence of two Brønsted-bound PPh_3 peaks at 11.1 and 14.8 ppm in ^{31}P MAS NMR is strongly supported by the above theoretical results.

4.3. Quantum Mechanical Calculation. It is well-known that the most fundamental problem in the chemistry of solid acids is determining the degree of proton transfer from a Brønsted acid to various adsorbed bases. After a molecular mechanical geometry optimization, more accurate quantum mechanical calculations were performed to further study the energetics of proton transfer from the Brønsted acid sites at the openings of the external surface pocket of MCM-22 zeolite to the probe molecules and the structures of acid−base complexes.

Because T1 and T4 sites had similar environments in the MCM-22 zeolite, we chose only the T4 site to perform the calculation with a reduced calculation time. Around the T4 site, there are three inequivalent framework oxygen atoms, O3, O6, and O7, that can be bound with a proton to form a hydroxyl. Because only the proton connected with O3 can interact with the P atoms of probe molecules according to the above molecular mechanical simulations, and the energy of Al substitution is a minimum when the proton is connected with O3,[25,26] our cluster models were focused on the Al4−O3(H)−Si1 site. During optimization, the dependences of the structure and interaction energy on the cluster model and density functional were all considered. The results are summarized in Table 1, Table 2 and Figure 4,

When a probe molecule approaches a Brønsted acid site, there are three general reactions that will happen between an acid (ZH) and a basic probe molecules (P):[40] (1) forming a "covalent" structure (ZH···P) (the proton is still attached to the bridging

TABLE 1: Optimized Bond Lengths and Interaction Energies between PPh_3 and MCM-22 Zeolite Cluster

	r(O−H) (Å)		r(P−H) (Å)		r(Al−P) (Å)		E_{energy}[a] (hartree)		ΔE[b] (kJ/mol)	
functionals	PWC	BLYP	PWC	BLYP	PWC	BLYP	PWC	BLYP	PWC	BLYP
model A-PPh_3	1.078	1.029	1.908	2.157	3.908	4.434	−2730.6709780	−2745.8313581	82.12	27.88
Model B-PPh_3	1.104	1.883	1.895	1.438	4.063	4.273	−3823.7674401	−3843.4518672	91.83	307.64
model $A^{netural}$	0.978	0.974					−1701.7056977	−1709.5510795		
model $B^{netural}$	0.979	0.976					−2794.7984580	−2807.1676250		

[a] E_{energy} represents the calculated total energy of complex. [b] ΔE represents the interaction energy of complex.

TABLE 2: Calculated Proton Affinity (PA) of Zeolite and Probe Molecules

	functional	$E^a_{neutral}$ (hartree)	E^b_{ionic} (hartree)	PA[c] (kcal/mol)	PA^{exp} (kcal/mol)
model A	PWC	−1701.7056977	−1701.2305554	298.16	
	BLYP	−1709.5510795	−1709.0679489	303.17	
model B	PWC	−2794.7984580	−2794.3271620	295.74	
	BLYP	−2807.1676250	−2806.6892074	300.21	
PPh_3	PWC	−1028.9339728	−1029.2990373	229.08	232.74
	BLYP	−1036.2696499	−1036.6453723	235.77	

[a] $E_{neutral}$ represents the calculated energy of the neutral fragment. [b] E_{ion} represents the calculated energy of the ionic fragment. [c] PA represents the calculated proton affinity. [d] PA^{exp} represents the experimental proton affinity.

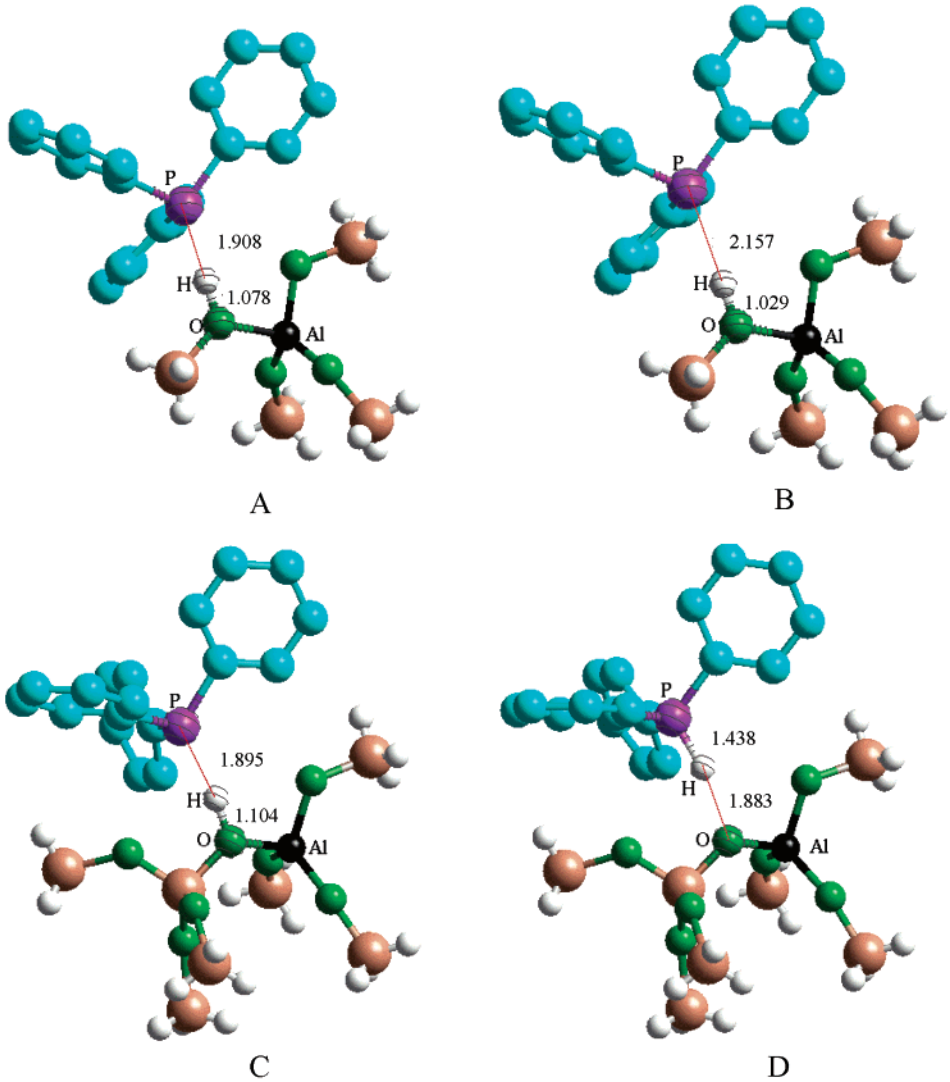

Figure 4. Structures of PPh_3−MCM-22 complexes. The H atoms of probe molecules are omitted for clarity. (A) represents the optimized structure with model A by the local PWC functional. (B) represents the optimized structure with model A by the nonlocal BLYP functional. (C) represents the optimized structure with model B by the local PWC functional. (D) represents the optimized structure with model B by the nonlocal BLYP functional.

oxygen of the zeolite but has a strong hydrogen bond with the probe molecule), (2) forming an "ionic" structure($Z^-\cdots HP^+$) (the proton has been transferred from the zeolite to the probe molecule stabilized by the Coulombic interaction and hydrogen bonding), and (3) forming a covalently bound onium ion complex. In this section we will discuss the dependence of the

structure of acid−base complexes on the cluster model and the density functional.

(A) Effect of the Cluster Model. From Table 1 and Figure 4, we can see that when using model A, only "covalent" structures between the probe molecules and zeolites were formed by both the local PWC functional and the nonlocal BLYP functional. The strength of hydrogen bonds between the protonic H atoms and the P atoms of probe molecules was quite large. The bond length between O and H increased more than 0.04 Å by the nonlocal BLYP functional (and even about 0.1 Å by the local PWC functional), as compared with the bond length of the bare zeolite. When changing the model from A to B, the situation was different. The bond length between the protonic H atom and the framework bridge O atom was increased from 1.078 to 1.104 but not transferred to PPh_3 by using the local PWC functional. However, when the local PWC functional was changed to the nonlocal BLYP further, the O−H bond length increased to an even greater extent, even leading to the breaking of the O−H bond and the formation of P−H bond simultaneously. Thus, the protonic H atom was transferred to the probe molecule, resulting in the "ionic" structure between PPh_3 and the zeolite. The calculation results implied that the neutral complex should be more stable than the "ionic" structure by using cluster model A. However, by using cluster model B in the calculations, the "ionic" structure was found to be more stable. The result was in agreement with the case of trimethylphosphine bound to the HY zeolite.[22] Moreover, after the formation of the "ionic" structure, large local rearrangement occurred near the Al ion. The aluminum and silicon tetrahedron became more symmetrical, similar to the structures obtained from the optimization of the bare zeolite anion.

In this section, the proton affinity (PA) of the zeolite was also calculated to explain the effect of cluster models on the structures of the complexes. The PA was reasonably approximated by the reaction $ZH \rightarrow Z^- + H^+$. The zero point vibrational energy differences and temperature effects were neglected, because they had little effect on the tendency in acidity for similar molecules. From the calculated results (see Table 2), we found that when changing the zeolite cluster model from $H_3Si-HO-Al(OSiH_3)_3$ to $(H_3SiO)_3Si-HO-Al(OSiH_3)_3$, the PA values of the zeolite were decreased by more than 2 kcal/mol on both the local PWC functional and the nonlocal BLYP functional. The difference in acidity based on the two models was due to the changes in the electrostatic field surrounding the acid site as the additional three O atoms, three Si atoms, and six H atoms were added in model B. The long-range electrostatic interactions would tend to stabilize the anion more than the neutral ones, and hence would decrease the PA values of the zeolite.[41] The cluster models with low PA values were better proton donors, and thus had higher Brønsted acidity. Thus, the cluster model B had a greater tendency to form the "ionic" structure than the cluster model A. The other reason for the formation of the "ionic" structure by using cluster model B may lie in the number of framework atoms of the cluster model. In cluster model B, there were more framework atoms than in cluster model A, which would lead to multiple interactions between PPh_3 and the zeolite cluster models, thus increasing the stability of the "ionic" structure. Lunsford[42] had observed that for nonproton-decoupled ^{31}P MAS NMR spectra of $(CH_3)_3P$ adsorbed on H−Y zeolite, the solo peak of the H−Y Brønsted site in the decoupled spectrum can be split into to a double-peak, indicating that a reaction (instead of weak interaction) is occurs for $(CH_3)_3P$ and the Brønsted sites in the zeolite. The current ionic model shows that the Brønsted proton has been transferred from the oxygen bridge to the phosphorus atom of the probe molecule, which is in good agreement with the result of Lunsford, etc.

(B) Effect of the Density Functional. Just as we have discussed before, the structures of the acid−base complex were also affected by the different density functionals. The local density functional depends only on the electron density, whereas the nonlocal density functional depends on the electron density as well as its gradient. The local density functional can be used to quite accurately predict the structures, vibrations, and relative energies of covalent systems. However, if weak bonds such as hydrogen bonds are present, then bond energies can be seriously overestimated. In cluster model A, the local PWC method overestimated the energies of the hydrogen bonds between protonic H atoms and P atoms of the probe molecules, resulting in a decrease of the bond lengths of P−H and an increase in the O−H bond lengths, when compared to the results obtained by the nonlocal BLYP functional. Due to the formation of the "ionic" structure in cluster model B, the local PWC functional overestimated the energies of the hydrogen bonds between the bridging O atoms and H atoms transferred to the probe molecules, resulting in the shortening of the O−H length and the stretching of the P−H bond lengths. Therefore we believed that more reliable structures would be obtained by the nonlocal BLYP functional.

5. Conclusions

In this work, the acidity on the external surface of the MCM-22 zeolite was studied by theoretical calculations combined with ^{31}P magic angle spinning (MAS) NMR experiment. Results are summarized as follows:

(1) The ^{31}P MAS NMR spectrum of triphenylphosphine adsorbed on the MCM-22 zeolite, and the XRF (X-ray fluorescence) element analysis showed that there were about 6% Brønsted acidic sites distributed on the external surface. Because the size of PPh_3 is larger than that of the 12-MR surface pocket, the ^{31}P MAS NMR experiment only detected a portion of the Brønsted acid sites on the external surface pocket of MCM-22 zeolite.

(2) Molecular mechanical simulations revealed that the probe molecules were too large to completely enter into the 12-MR pocket of the MCM-22 zeolite. They preferred to locate at the openings of the external surface pockets, with one alkyl inserting into the pockets of the supercage, whereas the others remained outside. The calculation results indicated that the 6% Brønsted acid detected by PPh_3 adsorption followed by ^{31}P MAS NMR experiment and XRF element analysis arose from the Brønsted acid sites at the mouth openings of the external surface pockets of the MCM-22 zeolite.

(3) The structures and interaction energies of the acid−base complexes were calculated by the DFT method. The calculation results indicated that after sorption of the probe molecules at the openings of the 12-MR external surface pockets of the MCM-22 zeolite, the protonic H atoms were transferred to PPh_3 and the "ionic" structure was formed. Because the Brønsted acidity was associated with the ability of transferring protons, the calculation results can give a qualitative understanding of the acidic strength at the openings of external surface pockets of the MCM-22 zeolite.

(4) The cluster models have a strong influence on the calculated results. Because of the long-range electrostatic interaction, cluster model B was more acidic and was capable of estimating the structure and energies of the acid−base complexes with higher reliability.

(5) The density functional also affected the calculated results. As the local functional only depends on the electron density, the local PWC functional would overestimate the hydrogen bond, thus predicting significantly larger values for the interaction energies between probe molecules and the zeolite, as compared to the nonlocal BLYP functional.

(6) The last and the most important was that the theoretical calculations provided structural support to the interpretation of experiment and they perfectly agree with the result of experiment which can be illustrated from three aspects below at least. (I) The calculation result has concluded that only parts of the acid sites are accessible to large probe molecules, confirming the result that only 6% Brønsted acid sites are detectable by ^{31}P MAS NMR with PPh_3 as the probe molecule. (II) Periodic MM calculation indicated that PPh_3 was able to adsorb on T1 and T4 sites, which are the most possible sites for the Al introduced into the zeolite lattice. The existence of two Brønsted-bound PPh_3 peaks at 11.1 and 14.8 ppm in ^{31}P MAS NMR was strongly supported by the above theoretical results. (III) It has been demonstrated by Lunsford, etc.[42] that for the non-proton-decoupled ^{31}P MAS spectrum of H−Y zeolite/$(CH_3)_3P$ complex, the solo peak of the Brønsted site of H−Y zeolite can be split into to a double-peak, showing that the proton of the Brønsted site haw been transferred to the probe molecule, which was in good agreement with the current DFT result; i.e., the ionic structure was the right structure for the probe−zeolite complex.

Acknowledgment. This work was supported by the National Natural Science Foundation of China (Key Program: No. 90206036) and the Ministry of Science and Technology of China (National Key Project of Fundamental Research: G1999022406).

References and Notes

(1) Rubin, M.; Chu, P. *U.S. Patent* **1990**, 4,954,325.
(2) Leononwica, M. E.; Lawton, J. A.; Rubin, M. K. *Science* **1994**, *264*, 1910.
(3) Aseni, A.; Corma, A.; Martinez, A. *J. Catal.* **1996**, *158*, 561.
(4) Ravishankar, R.; Sivasanker, S. *Appl. Catal. A* **1996**, *142*, 47.
(5) Corma, A.; Gonzàlez-Alfro, V.; Orchillès, A. V. *Appl. Catal. A* **1995**, *129*, 203.
(6) Corma, A.; Martinez-Triguero, J. *J. Catal.* **1997**, *165*, 102.
(7) Ravishankar, R.; Joshi, P. N.; Tamhankar, S. S.; Sivasanker S.; Shairalkar, V. P. *Adsorp. Sci. Technol.* **1998**, *16* (8), 607.
(8) Prakash, A. M.; Wasowica, T.; Keven, L. *J. Phys. Chem. B* **1997**, *101*, 1985.
(9) Coma, A.; Corell, C.; Pérez-Pariente, J.; Guil. J. M.; Guil-López, R.; Nicóoulos, S.; Calbet, J.; Vallet-Regi, M. *Zeolite* **1996**, *16*, 7.
(10) Wu, P.; Komatsu, T.; Yashima, T. *Micropor. Mesorpor. Mater.* **1998**, *22*, 343.
(11) Lawton, S. L.; Leonowica, M. E.; Partridge, R. D.; Chu, P.; Rubin, M. K. *Micropor. Mesopor. Mater.* **1998**, *23* (1−2), 109.
(12) Weitkamp, J.; Weip, U.; Ernst, S. Catalysis by Microporous Materials. *Stud. Surf. Sci. Catal.* **1995**, *94*, 363.
(13) Cheng, J. C.; Fegnan, T. F.; Beck, J. S.; Huang, Y. Y.; Kalyanaraman, M.; Kowalski, J. A.; Loehr, C. A.; Mazzone, D. N. *Stud. Surf. Sci. Catal.* **1999**, *121*, 53.
(14) Nicolopulos, S.; González-Xalbet, J. M.; Vallet-Regi, M.; Coma, A.; Corell, C.; Guil. J. M.; Pérez-Pariente, J. *J. Am. Chem. Soc.* **1995**, *117*, 8947.
(15) Roque-Malherbe, R.; Wendelbo, R.; Mifsud, A.; Corma, A. *J. Phys. Chem.* **1995**, *99*, 14064.
(16) Meloni, D.; Laforge, S.; Martin, D.; Guisnet, M.; Rombi, E.; Solinas, V. *Appl. Catal. A* **2001**, *215*, 55.
(17) Du, H. W.; Olson. D. H. *J. Phys. Chem. B* **2002**, *106*, 395.
(18) Corma, A.; Diaz, U.; Fornés, V.; Guil, J. M.; Martínez-Teiguero, J.; Creyghton, E. J. *J. Catal.* **2000**, *191*, 218.
(19) Lunsford, J. H.; Rothwell, W. D.; Shen, W. *J. Am. Chem. Soc.* **1985**, *107*, 1540.
(20) Baltusis, L.; Frye, J. S.; Maciel, G. E. *J. Am. Chem. Soc.* **1987**, *109*, 40.
(21) Sheng, T. C.; Gay, I. D. *J. Catal.* **1994**, *145*, 10.
(22) Kao, H.-M.; Liu, H. M.; Jiang, J.-C.; Lin, S.-H.; Grey, C. P. *J. Phys. Chem. B* **2000**, *104*, 4923.
(23) Ehresmann, J. O.; Wang, W.; Herreros, B.; Luigi, D.-P.; Venkatraman, T. N.; Song, W. G.; Nicholas. J. B.; Haw, J. F. *J. Am. Chem. Soc.* **2002**, *124*, 10868.
(24) Sastre, G.; Fornes, V.; Corma, A. *J. Phys. Chem. B* **2000**, *104*, 4349.
(25) Zhou, D. H.; Wang, Y.; Ma, D.; Bao, X. H. *Chem. J. Chin. Univ. (8th Quantum Chem. Mtg.) 2002*, 207−211.
(26) Zhou, D. H.; Wang, Y.; Bao, X. H. *J. Chem. Phys.*, submitted for publication.
(27) Chen, C. S. H.; Schramm. *Micropor. Mater.* **1996**, *7*, 125.
(28) Cheng, M. J.; Tan, D. L.; Liu, X. C.; Bao, X. H.; Lin, L. *Micropor. Mesopor Mater.* **2001**, *42*, 307.
(29) Sastre, G.; Corma, A. Chem. *Phys. Lett.* **1999**, *302*, 447.
(30) Simperler, A.; Bell, R. G.; Philippou, A.; Anderson, M. W. *J. Phys. Chem. B* **2002**, *106*, 10944.
(31) Corrêa, R. J.; Mota, C. J. A. *J. Am. Chem. Soc.* **2002**, *124*, 3484.
(32) Meier, W. M.; Olson, D. H.; Baerlocher, C. *Altas of Zeolite Structure Type*, 4th ed.; Elsevier: Amsterdam, 1996. Also on http://www.iza-structure.org/databases/.
(33) CERIUs2, Version 4.2, Dmol 3, Molecular Simulations Inc., 2000.
(34) Catlow, C. R. A.; Ackermann, L.; Bell, R. G.; Cora, F.; Gay, D. H.; Nygren, M. A.; Pereira, J. C.; Sastre, G.; Slater, B.; Sinclair, P. E. *Faraday Discuss.* **1997**, *106*, 1.
(35) Gordon, M. S. *Chem. Phys. Lett.* **1980**, *76*, 163.
(36) Hehre, W. J.; Ditchfield, R.; Pople, J. A. *J. Chem. Phys.* **1972**, *56*, 2257.
(37) Hu, B.; Gay, I. D. *Langmuir* **1999**, *15*, 477.
(38) Hou, T. J.; Zhu, L. L.; Xu, X. J. *J. Phys. Chem. B* **2000**, *104*, 9356.
(39) Ocakoglu, R. A.; Denayer, J. F. M.; Marin, G. B.; Martens, J. A.; Baron, G. V. *J. Phys. Chem. B* **2003**, *107*, 398.
(40) Song, W. G.; Nicholas, J. B.; Haw, J. F. *J. Am. Chem. Soc.* **2001**, *123*, 121.
(41) Stave, M. S.; Nicholas, J. B. *J. Phys. Chem. B* **1995**, *99*, 15046.
(42) Rothwell, W. R.; Shen, W. X.; Lunsford, J. H. *J. Am. Chem. Soc.* **1984**, *106*, 2452.